Talanta Open 11 (2025) 100440

Contents lists available at ScienceDirect

Talanta Open

journal homepage: www.sciencedirect.com/journal/talanta-open

Geographic determination of *Pinus ponderosa* using DART TOFMS, ICP-MS, and LIBS handheld analyzer

Erin R. Price [a,*], Kierra R. Cano [a], Caelin P. Celani [b], Helder V. Carneiro [b], Karl S. Booksh [b], James A. Jordan [c], Pamela J. McClure [d], Megahn H. Pinedo [a], Michael E. Ketterer [e], Kent M. Elliott [a], Tyler B. Coplen [c], Edgard O. Espinoza [d]

[a] US Forest Service International Programs Wood Identification and Screening Center, Ashland, OR, USA
[b] University of Delaware, Newark, DE, USA
[c] US Geological Survey, Reston, VA, USA
[d] US Fish and Wildlife National Forensics Laboratory, Ashland, OR, USA
[e] Northern Arizona University, Flagstaff, AZ, USA

ARTICLE INFO

Keywords:
Timber provenance
Machine learning
Trace elements
Ambient ionization
Timber trade
Wood identification

ABSTRACT

Due to legal requirements on international imports, it is important for law enforcement and regulatory agencies to identify the geographical provenance of timber. Current methods for geographic identification utilize data generated by direct analysis in real time time-of-flight mass spectrometry (DART TOFMS), genetics, and isotope-ratio mass spectrometry (IRMS), but identification methods based on genetics and IRMS data require months to years to create usable databases. This study used machine learning algorithms to compare the results of DART TOFMS, inductively coupled plasma mass spectrometry (ICP-MS), and a handheld laser-induced breakdown spectroscopy (LIBS) analyzer for use in geographic identification of five populations of *Pinus ponderosa* spaced between 14 to 72 km apart. The results of the study showed comparable performances from machine learning algorithms applied to the ICP-MS and LIBS data with accuracy and kappa values over 90% while the DART TOFMS had an accuracy of 76% and a kappa value of 70%. This study demonstrated that data from the LIBS handheld analyzer is a viable and intriguing alternative to ICP-MS and DART TOFMS analyses in generating training databases and further indicates that trace elemental analysis via ICP-MS is a promising method for generating databases used to identify the origin of timber.

Introduction

As the global trade in timber continues to expand [1,2], law enforcement and regulatory agencies are turning their attention to identifying not just what timber species are found in trade, but where they come from as well. Several international import legality requirements, such as those included in the 2008 amendments to the U.S. Lacey Act, require accurate declaration of geographic origin for wood products [3]. However, inspection agencies lack adequate tools to assess these declarations for accuracy, unless they contain obvious misrepresentations [4]. Furthermore, certain economies are instituting geolocation requirements as part of sustainability initiatives, such as the European Union Deforestation Regulation [5].

Previous research demonstrates that tree populations are influenced by available nutrients, climate, habitat, and geography and this variability can be detected using laboratory tools [6–8]. Indeed, researchers have looked to a series of different analytical techniques to answer the question of why intraspecies variation is found in populations with different geographic origins. Squillace [9] theorized that morphological differences found in 54 stands of *Pinus elliottii* were based on pressure from climate and environmental factors in addition to latitude. Studies involving metabolites have also been conducted to explain intraspecies variation: in 1971, Stepanov & Dubovenko [10,11] used gas chromatography to show that the amount of α-pinene in *Pinus sibirica* changed substantially between trees sampled from two locations within Siberia, while Zavarin et al. [12] found that camphene and 3-carene could be used to differentiate populations of *Abies concolor* via gas-liquid chromatography.

Currently, the primary methods of generating training databases for geographic origin identification of timber are genetics, isotope-ratio

* Corresponding author.
E-mail address: erinmcclureprice@gmail.com (E.R. Price).

https://doi.org/10.1016/j.talo.2025.100440
Received 16 September 2024; Received in revised form 25 February 2025; Accepted 19 March 2025
Available online 19 March 2025
2666-8319/© 2025 The Authors. Published by Elsevier B.V. This is an open access article under the CC BY-NC-ND license (http://creativecommons.org/licenses/by-nc-nd/4.0/).

mass spectrometry (IRMS), and direct analysis in real time time-of-flight mass spectrometry (DART TOFMS). Studies using genetics have been highly successful [13,14], and ongoing research into utilizing IRMS data shows the method has potential [15–17]. However, both genetics and IRMS require months to years to create usable databases, and the cost per sample analysis is high. This suggests that both methods could be difficult to implement in regions where deforestation is most active and local economies may not support the costs [18].

Studies using DART TOFMS have shown that it is a powerful forensic tool that can be used for myriad applications from drug and explosive analysis to species identification through timber and keratin analysis [19]. It has also been used to detect geographic signals in select timber species [20–22]. However, DART TOFMS instrumentation is not available worldwide. To account for limitations in method availability, we chose to evaluate two additional analytical techniques, which may be more easily obtained in other regions: a handheld laser-induced breakdown spectroscopy (LIBS) analyzer and inductively coupled plasma mass spectrometry (ICP-MS).

ICP-MS is often used when trace elemental analysis is required due to the technique's ability to determine the concentration of a range of metals down to trace and ultra trace, defined as parts per million – parts per trillion (ppm-ppt), detection limits [23]. More recently, ICP-MS has been gaining popularity as a method to trace and authenticate agricultural product origins [24,25]. Alaimo et al. [26] used ICP-MS to determine trace element concentrations, such as vanadium, molybdenum, lead, and zirconium, present in Sicilian fungi. They ultimately found that the concentrations of these elements were species- and grow site-dependent. These findings were in agreement with those of Mazarakioti et al. [25], who noted that the elemental concentration of soil directly influences the growth of agricultural products, which suggests that the elemental composition of a plant can be linked to its origin. In addition, Boeschoten et al. [27] utilized ICP-MS to demonstrate a direct relationship between the relative elemental compositions of soil and those of sapwood and heartwood. This finding suggests the detectability of a connection between environmental element concentrations in soil and timber.

LIBS handheld analyzers are gaining in popularity due to their capability to rapidly obtain both qualitative and quantitative in situ concentrations from materials with little to no sample preparation and negligible sample destruction. The traditional applications for LIBS analyzers have been elemental analyses of metallurgical materials [28–30] and geological samples [31,32], but recent research has shown that the LIBS is a versatile tool that can be used for a variety of analyses including soils [33–36], and even plants [37–39].

Few studies are available that explore LIBS as a tool for use in geographic origin identification of plants; however, the research that is available shows that the method has promise. Baskali-Bouregaa et al. [40] found that the regional origin of tea could be identified using LIBS data combined with inductively coupled plasma high resolution mass spectrometry (ICP-HRMS) data, while Gyftokostas et al. [41] found that they could classify the geographic region of olive oil based on LIBS spectral data. El-Deftar et al. [42] showed that they could separate *Cannabis* grown with six different liquid nutrients, suggesting that available nutrients substantially alter the elemental composition of a plant. Furthermore, the study by El-Deftar et al. [42] found that the LIBS results were consistent with those of ICP-MS and laser ablation ICP-MS, indicating that the instrument could be an effective and field-deployable forensic tool.

Each of the three aforementioned instruments have different advantages based on the type of data that can be collected, but the main questions this study aimed to answer were: can the hand-held LIBS compare to the lab-restricted ICP-MS and DART TOFMS in terms of efficiency and reliability for use in quickly and accurately collecting concentration data that can be used for the identification of the origin of a wood sample, and which is the best tool for the purpose of origin identification of wood. The goal of this study was to directly compare the results from three different analytical techniques—DART TOFMS, LIBS, and ICP-MS—through machine learning algorithms with the purpose of evaluating each technique for use in geographic origin identification. For this purpose, we collected core samples from *Pinus ponderosa* trees growing in five discrete populations in southern Oregon to (1) test the resolution of each method (i.e., what distance between populations will allow for separation), and (2) compare the reliability of each method.

Methods

Sample collection

Genetic research on native populations of *P. ponderosa* has revealed that the species likely consists of four disparate species, *P. ponderosa, P. benthamiana, P. brachyptera*, and *P. scopulorum*, rather than one [43], and analysis of monoterpene levels in *P. ponderosa* suggested that there were five distinct growing regions that could be used to classify the species [44]. To account for potential subspecies or variants, the samples collected for this study were taken from a range that had been previously determined by Willyard et al. [43] and Smith [44] to be made up of conspecific individuals.

Using increment borers (Haglöf 2-Thread, 14" x 0.200"), 20 to 23 samples of individual *P. ponderosa* trees were collected from five locations in southern Oregon (Fig. 1) for a total of n = 106. Each core sample contained sapwood and heartwood. The locations in southern Oregon were abbreviated as follows with the associated most-granular hydrologic unit code (HUC12) designated by the U.S. Geological Survey (USGS): Jacksonville (JV, 171003080112), Lithia Park, Ashland (LP, 171003080106), Colestin Road, Colestin (CR, 180102060602), Howard Prairie Resort Campground (HP, 180102060401), and Pelican Guard Station (PG, 180102030203)[45]. Distances among locations ranged from approximately 14 to 72 km. Although all samples were collected in the proximity of Ashland, Oregon, three sample locations are technically in the HUC2 California Region (CR, HP, PG) and two locations are in the HUC2 Pacific Northwest Region (JV and LP).

Samples were stored in aluminum foil and dried at 30°C for two weeks prior to analysis. Geographic coordinates for each sample can be found in Supplemental Table 1.

DART TOFMS

Mass spectra from the *P. ponderosa* cores were collected using a DART ion source (IonSense, Saugus, MA. USA) coupled to a time-of-flight mass spectrometer (AccuTOF 4G, JEOL USA, Peabody, MA. USA). Operational instrument settings for DART TOFMS data collection can be found in McClure et al. [46]. A small subsample "coin" was sliced from the heartwood of each core sample using a razor blade and a total ion chromatogram (TIC) for each core was collected by holding the subsample with forceps in the sample gap of the instrument, within a stream of helium gas heated to 350°C. Poly(ethylene) glycol 600 (Sigma-Aldrich, St. Louis, MO, USA), diluted with methanol (1:10 volume ratio), was used as the calibrant. Core samples were analyzed in batches of ten, with a calibrant spectrum collected at the beginning, middle, and end of each batch. The calibrant was collected by dipping the closed end of a capillary tube into the solution and holding it in the sampling gap. Mass spectra were produced by averaging the individual subsample TICs and exporting each one as centroided text files using the DART TOFMS accompanying msAxel software (version 1.05.2) [47].

The digitized TOF spectra as saved by the DART were not naturally aligned for matrix based, machine learning algorithms. Only the intensity of ion currents above a certain threshold were recorded and those were time-stamped to the nearest 0.001 m/z based on the poly(ethylene) glycol 600 calibration. Consequently, the TOF spectra were binned in 0.1 m/z windows to digitally align the ion peaks while preserving much of the true ~0.01 m/z instrumental resolution. Entries without a

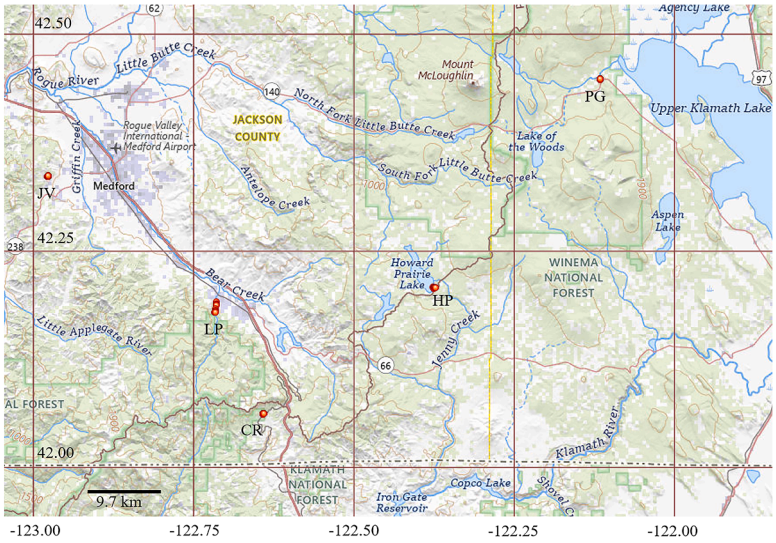


Fig. 1. Map of each Pinus ponderosa sampling location indicated by red dots. Hydrologic Unit Code (HUC12), longitude, and latitude were recorded for each tree core. Each abbreviation corresponds to a given location designated by the HUC12 name and number: Jacksonville (JV, 171003080112), Lithia Park, Ashland (LP, 171003080106), Colestin Road, Colestin (CR, 180102060602), Howard Prairie Resort Campground (HP, 180102060401), and Pelican Guard Station (PG, 180102030203). Map data from the U.S. Geological Survey National Map Viewer [45].

recorded *m/z* value were assigned a value of 0. For multivariate analyses, variable selection was performed by identifying bins that had non-zero signals for at least 80, 90, and 106 of the 106 spectra. Thus, the impact of assigning missing values the intensity of "zero" was minimized.

ICP-MS

The remaining material from each core sample, consisting of both sapwood and heartwood, was divided into smaller pieces to fit in individual 40-mL-Pyrex-VOA bottles. Each sample was converted to ash by placing the bottles in a muffle furnace (Thermolyne 1300, Dubuque, IA, USA) and heating to 600°C for 10 hr. Ash samples were then transferred to tared 15-mL-polypropylene-centrifuge tubes. Net sample mass was recorded to the nearest 0.0001 g (Supplemental Table 1). In addition to the 106 samples, five reagent blanks were prepared in 15-mL tubes from the same lot. Thereafter, 5 mL of 8 M aqueous nitric acid was added; the tubes were tightly capped, and the mixtures were heated in a convection oven at 75°C for 2.5 hr. For most of the samples, dissolution was observed to be complete (i.e., no un-dissolved solids were evident); however, five samples appeared to have been incompletely burnt to ash, and these samples produced solutions with a pale green-brown color and an observable solid residue; these samples were the following: JV10, JV12, JV13, JV15, and JV17.

Following the dissolution procedure, 1.00 mL of each sample solution was diluted by addition of 4.00 mL of an internal standard solution, which contained 10 μg/L each of rhodium (Rh) and iridium (Ir) in 0.5% aqueous nitric acid by volume. A tuning solution was prepared that contained 5 μg/L of each of the following elements: lithium, cobalt, indium, barium, cerium, bismuth, and uranium. An aliquot of the 5 μg/L of tuning solution was prepared by mixing 25 μL of a 1000-μg/L stock tuning solution (CPI International, Santa Rosa, CA., USA), 0.975 mL of 8-M nitric acid (ACS Certified Plus Grade, Fisher Chemical Co., Waltham, MA., USA), and 4.00 mL of the rhodium/iridium internal standard solution.

Analysis was performed using a Thermo X2 quadrupole ICP-MS system (Thermo Fisher Scientific Corp., Eugene, OR., USA). The instrument was used with a horn-shaped (standard factory) Peltier-cooled spray chamber held at 5°C, and it employed a concentric glass nebulizer supplying sample at the rate of ~1.0 mL/minute with a peristaltic pump. Samples were introduced and runs were initiated manually. Between samples, rinsing was accomplished using the next sample in the analytical queue, and at least 20 s of steady-state response was observed prior to commencing collection of the mass spectral scan. Mass spectral ion intensities were collected in the Thermo X2 "survey scan" mode, with a series of n = 50 rapid, 1.3 s sweeps being conducted between 5 and 245 *m/z*. One scan was conducted per sample; repeat collections of spectra for n = 5 samples were also performed at the end of the analysis. Approximately every 20 samples, spectra were also collected of the 5-μg/L tuning solution, followed by the reagent blank; the latter was diluted in the same manner as the wood core ash samples by addition of 4.00 mL of an internal standard solution.

LIBS

No additional sample preparation was conducted for the *P. ponderosa* cores. A SciAps Z-300 LIBS Analyzer (Boston, MA, USA) was used for data collection, which contained a 1064-nm laser source operating at 5-6 mJ/pulse and a 50-Hz repetition rate. The wavelength calibration for the instrument was performed internally on 316 stainless steel, and qualitative sample spectral data were collected. The laser spot size was approximately 50 μm in diameter, and spectra were collected from heartwood sections of the *P. ponderosa* cores. The LIBS was set to collect eight spectra from a single location in a 4 × 3 raster pattern per sample under a purge of high purity grade argon to increase signal intensity and eliminate the effect of atmospheric gasses and humidity. At each location of the 4 × 3 grid, two cleaning pulses from the laser were used to ablate contamination off the surface; then, optical emission following eight laser pulses were averaged to yield a single LIBS spectrum per location. This resulted in 12 recorded LIBS spectra per pine sample.

Due to significant baseline in portions of the LIBS spectrum, an asymmetric least squares algorithm was applied piecewise to each spectrum such that baseline effects were approximately linear within each region (Eilers 2003). The wavelength regions chosen for baseline correction were as follows: 188.0 – 324.6 nm, 324.6 – 365.0 nm, 365.0 – 390.5 nm, 390.5 – 416.0 nm, 416.0 – 441.5 nm, 441.5 – 467.0 nm, 467.0 – 492.5 nm, 492.5 – 518.0 nm, 518.0 – 569.0 nm, 569.0 – 620.0 nm, and 620.0 – 949.5 nm. For each region, the second derivative constraint, λ, that controls smoothness was set to 10 and the positivity constraint, p, that controls asymmetry was set to 0.05. After baseline correction each spectrum was normalized to unit area (divide each spectrum by its sum). The spectra were then reduced from 23,431 variables to 1080 variables

by manually identifying the location of LIBS peaks common across the samples. After variable selection, the absolute value and square root transformation were applied sample-wise to all LIBS spectra to emphasize low-intensity spectral features.

Machine learning

All analyses were performed in R [48] using the RStudio [49] operating interface. The caret package [50] was employed to control the workflow of each classification method and to assure that each classification method interacted with the data equivalently. Additional packages 'doParallel' [51], 'signal' [52], 'readxl' [53], 'baseline' [54], 'discretization' [55], 'dplyr' [56], and 'stats' [48] were included for data management.

Up to three strategies to best condition the data for multivariate classification models were considered for all data sets. A minimalist approach was tested where each variable was scaled to unit variance. To better conform with the underlying assumption of a normal distribution of observations of the multivariate models, each variable of the mass spectra was normalized by a Box-Cox transformation [57,58] prior to scaling to unit variance. This theoretically minimizes the deleterious effect of extreme outliers. This normalization was not needed for the LIBS variables, which were scaled to unit variance without a Box-Cox transformation. Also, for classification models, supervised discretization [55] of each variable based on sample class membership was investigated. The class-attribute interdependence maximization (CAIM) algorithm was employed to guide discretization [59]. Supervised discretization offers some value of reducing extreme observations and potentially eliminates sources of variance unrelated to differentiation among the classes [59,60].

To best compare the methods and estimate the efficacy of data from the three spectroscopic techniques for use in geolocation of the pine samples, the same procedure was applied to all three data sets for creating training and validation sets and for tuning the models with cross-validation. Ten training and ten validation sets were created with a random 80-20 data split by bootstrapped Latin partitions to maintain the identical class distributions in the training and validation sets with the caret [50] package's createDataPartition() function. The same random number generator seeds were employed for data sets from all three analyses. Method results are presented as an ensemble performance metric across all ten models/validation sets. Within each training set, cross-validation was performed with the 'repeatedcv' function in caret [50]. Twenty percent of the training set was removed, without replacement, to create five splits where 20% of the data was randomly omitted each time. This procedure was repeated ten times for ten different splits within each cross-validation loop. The model parameters with the lowest root mean squared error of cross validation (for quantitative models) or greatest Cohen's Kappa (for classification models) were accepted as optimized.

Partial least squares regression (PLSR) was employed to quantitatively determine the longitude and latitude from pine samples analyzed by the three different instrumental methods. Additionally, partial least squares discriminant analysis with a single model approach (PLS2-DA) [61] and Support Vector Machines (SVM) [62] were employed to classify the pine samples by HUC designation.

For an in-depth analysis of LIBS data, the elemental library, "LIBZ Database" in the Profile Builder software (SciAps, Boston, MA.), supplemented with the accompanying built-in NIST elemental lines, was used to manually identify peaks found within the dataset. Peaks were identified manually on a peak-by-peak basis, aiming to identify as many peaks as possible while minimizing erroneous identification through domain knowledge, i.e., rejecting peaks associated only with obscure elements unlikely to be found in hardwood samples like osmium. Because the observed LIBS spectrum is highly dependent upon plasma temperature, surrounding atmosphere, electron density, plasma opacity, and detector gating delay time, library searching for peak identification is difficult. Once LIBS lines were identified, neighboring pixels associated with the same peak were labeled as the same element, due to the collinear nature of neighboring pixels in spectroscopic data, thus giving wavelength ranges associated with each given elemental identification.

Variable importance in projection (VIP) scores were calculated to assess the influence of each variable on the final model. Ideally, the most important variables will be tied to the local geochemistry and shed light onto the differential soil and water chemistry among the locations. When the important variables span these elements, greater faith is placed in the model. On the other hand, when the most important variables in building a model are rare or esoteric elements, e.g., osmium and erbium, the final model is skeptically viewed as relying on chance correlations. Such *post-hoc* analyses allow the analyst to garner a functional understanding of the model's predictive reliability under the assumption that the model is properly tuned and validated through a scaled "percent importance" metric associated with each input variable.

Determining VIP scores is not straightforward. Many methods, such as PLS, have model-dependent importance metrics [63,64]. In PLS, variable importance us derived from the absolute value of the regression coefficients, weighted by the reduction in the sum of squares across the number of PLS components. Other methods, like SVM, have no model-dependent VIP scores. Here, model-agnostic approaches are required which estimate variable importance through variance-, permutation-, or shapely-based metrics. The varImp() [65] function in R determines the model-dependent VIP scores when possible. For models without dependent VIP scores, VIP scores are determined by locally-weighted polynomial regression which fits each variable to the desired output for regression applications or by calculating the area under the curve (AOC) of a receiver operating characteristic (ROC) curve – or a multi-class ambiguation of a ROC curve – for each variable relative to the desired classification output for classification applications.

Results

DART TOFMS: classification by HUC

Preliminary analyses of the 5-class model by PLS2-DA and SVM indicated that preprocessing the data by discretization returned better accuracy and larger kappa values than did preconditioning the data with a Box-Cox transformation or just normalizing each variable to unit standard deviation. Preliminary analyses also determined that selecting variables that were included in 90 of the 106 samples (487 m/z ratios) or in 80 of the 106 samples (643 m/z ratios) performed better than only using the variables present in all 106 samples (182 m/z ratios). In these cases, absent m/z ratios were imputed to be 0.

For PLS2-DA classification, the ten repetitions ranged from having 8-15 factors with 69.3% of variance explained. PLS2-DA and SVM, both using discretization, performed similarly according to cross-validation (CV) of the training set. T-tests were used to calculate probability (p) of CV outputs and showed no significant differences in accuracy ($p = 0.73$) and kappa ($p = 0.73$) between SVM and PLS2-DA. Similarly, regarding the validation set, there were no significant differences in accuracy ($p = 0.39$) and kappa ($p = 0.38$) (Table 1). Kappa values are related to accuracy, except the kappa values account for the expected accuracy achieved from random guessing. Consequently, a kappa of 0 indicates the model is no better that random chance and a kappa in the 0.7 to 0.8 range supports a strong, but not exceptional, model performance [66].

The confusion matrix for the PLS2-DA classification model (Table 2) shows a prominent off-diagonal structure where some classes are most likely to be misclassified as one or two other particular classes. Arranging the confusion matrix by ascending latitude (northing), one observes the superdiagonal and subdiagonal elements of the matrix show increased misclassifications, indicating that a given location is most likely to be misclassified as its next closest location, by latitude.

Table 1
Performance metrics for best classification models applied to the DART TOFMS, ICP-MS, and LIBS data. Mean and standard deviation values from 10 replicate re-samplings are presented.

	CV accuracy	CV kappa	Validation accuracy	Validation kappa
DART TOFMS				
PLS2-DA	0.83 ± 0.02	0.79 ± 0.02	0.76 ± 0.09	0.70 ± 0.11
SVM	0.83 ± 0.03	0.78 ± 0.04	0.73 ± 0.06	0.66 ± 0.08
ICP-MS				
PLS2-DA	0.85 ± 0.02	0.81 ± 0.02	0.93 ± 0.06	0.91 ± 0.07
SVM	0.85 ± 0.02	0.81 ± 0.02	0.88 ± 0.05	0.85 ± 0.07
LIBS				
PLS2-DA	0.842 ± 0.004	0.802 ± 0.005	0.84 ± 0.02	0.80 ± 0.02
SVM	0.918 ± 0.004	0.897 ± 0.004	0.92 ± 0.02	0.91 ± 0.02

Table 2
Confusion Matrix for 10 randomized PLS2-DA classification predictions with the DART TOFMS dataset. Each abbreviation corresponds to a given location designated by the HUC12 name and number: Jacksonville (JV, 171003080112), Lithia Park, Ashland (LP, 171003080106), Colestin Road, Colestin (CR, 180102060602), Howard Prairie Resort Campground (HP, 180102060401), and Pelican Guard Station (PG, 180102030203).

True Location Abbreviation						
Predicted Location Abbreviation	Predicted \ True	CR	HP	LP	JV	PG
	CR	30	9	1	0	0
	HP	9	24	7	0	0
	LP	0	1	35	5	0
	JV	0	0	0	31	7
	PG	1	1	0	6	31

Permuting the confusion matrix in order of longitude shows no trend in misclassifications. The confusion matrix for SVM analyses is qualitatively similar to the PLS2-DA confusion matrix.

Regression by longitude and latitude. PLSR of latitude and longitude against DART TOFMS returned a root mean square error of prediction (RMSEP) of 0.09 ± 0.04 and 0.38 ± 0.19, respectively, across 10 randomized calibration models. This corresponds to 10-km latitude and 31-km longitude accuracy. Tuned models required 3 factors for latitude which described 46.16% of variance, while longitude required an average of 3 factors which described 50.87% of variance. While both regression models are statistically significant versus "no model," plots of true versus predicted latitude (Fig. 2 a) and longitude (Fig. 2 c) indicate much better latitude resolution than longitude resolution. Predicted latitude (Fig. 2 b) density maps show the ability to resolve the two northernmost locations (PG and JV) from the three southernmost locations (LP, HP, and CR), but little discerning power within those two groups. Simultaneously, predicted longitude (Fig. 2 d) density maps for the five locations show substantial overlap in the predicted locations and only marginal ability to resolve the westernmost and easternmost locations.

ICP-MS: classification by HUC

With the ICP-MS data, PLS2-DA and SVM classification models employing either a Box-Cox transformation or discretization for preprocessing all performed equivalently. Consequently, the PLS2-DA model following a Box-Cox transformation was selected as most optimal due to its net simplicity compared to the other options (parsimony principle) bolstered by the observation that the predictive accuracy (p-value = 0.04 for PLS2-DA vs SVM) and kappa (p-value = 0.07 for PLS2-DA vs SVM) for this model were numerically the best. The PLS2-DA model performed with a predictive accuracy of 0.93 ± 0.06 and a predictive kappa of 0.91 ± 0.07 based on 10 randomized training and validation sets (Table 1). The PLS2-DA model repetitions used 10 factors which explained 82.09% of the variance. The confusion matrix for the PLS2-DA classification model shows most of the misclassified samples associated with LP, near the center of the map (Table 3).

Regression by longitude and latitude

PLSR models, following a Box-Cox transformation, against latitude and longitude using the ICP-MS data returned RMSEP of 0.08 ± 0.01 and 0.15 ± 0.02, respectively, across 10 randomized calibration models. This corresponds to 9-km latitude and 12-km longitude resolution at one standard deviation. Tuned models required an average of 4 factors for latitude and for longitude, explaining 56.32% and 58.18% of variance, respectively. depending on the randomized training set. Plots of predicted versus true latitude (Fig. 3 a) and longitude (Fig. 3 c) show a significant trend across the geospatial coordinates. However, the density plots of predicted latitude (Fig. 3 b) or longitude (Fig. 3 d) for each of the five illustrate that the models are truly only able to resolve three locations across the data – near the two extremes or in the middle. A close inspection of the modes in the longitude density plots shows the most frequently predicted locations of CR and LP reversed in their true order.

LIBS: classification by HUC

With the LIBS data, SVM classification models were found to provide better classification accuracy and kappa for prediction than PLS2-DA models ($p < 0.01$), which had 10 factors explaining 54.73% of the variance. SVM creates a more flexible, non-linear model than does the linear PLS2-DA. However, SVM requires a larger training set to realize this potential benefit. The ability of the hand-held LIBS to rapidly generate a large training set supports the use of SVM in this application. LIBS measures metal concentration in the samples as nutrients are absorbed. Each of the 12 locations analyzed on a core can be treated as independent samples because each location contains a snap-shot of a particular year's nutrient uptake. Additionally, preprocessing by normalization to unit variance performed equivalently to preprocessing by discretization ($p = 0.50$). Therefore, based on the parsimony principle, the best tuned model uses SVM on auto-scaled data to return a predictive accuracy of 0.92 ± 0.02 and a predictive kappa of 0.91 ± 0.02 (Table 1) based on 10 random re-samplings.

As would be expected for a model with a 0.92 accuracy and a 0.91 kappa, misclassification events are rare occurrences as evidenced in the confusion matrix for the SVM classification model (Table 4). The most confused locations, based on average misclassifications across 10 iterations, occur between CR and HP followed by CR and LP. Geospatially, these locations are the most proximate, with CR and LP being the most similar in both latitude and longitude, but CR and HP most similar in HUC area. This indicates that the LIBS signals convolute spatial position and mineralogic composition when used to identify provenance. This observation is corroborated by the fact that LP and CR are both fed by the Rogue River Watershed that is, in turn, fed by overflow from Crater Lake. Furthermore, CR is misclassified as LP over twice as frequently as the inverse, as explained by CR being located further down the watershed than LP. HP is located next to Howard Prairie Lake, which is fed by the Klamath River Watershed and has no connection to Crater Lake, indicating that misclassifications between HP and CR are not readily explained.

Regression by longitude and latitude

PLSR models, following normalization to unit standard deviation and unit variance, against latitude and longitude using the LIBS data returned RMSEP of 0.087 ± 0.004 and 0.130 ± 0.004, respectively, across 10 randomized calibration models. The models required 9 factors for latitude and 10 factors for longitude, with 52.29% and 53.83%

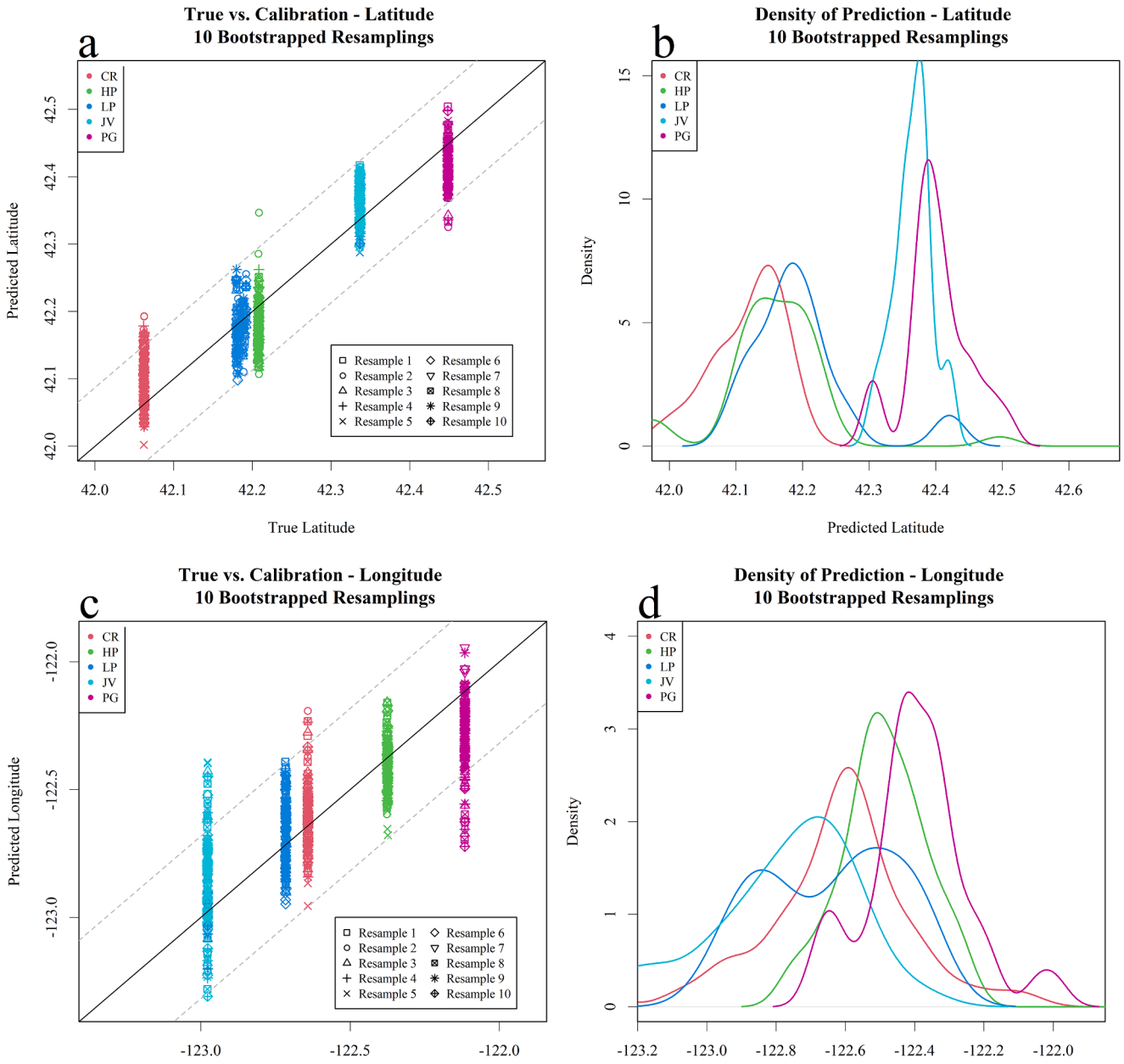


Fig. 2. PLSR models against latitude and longitude using the DART TOFMS data. RMSEP for latitude was 0.09 ± 0.04 and longitude was 0.38 ± 0.19 across 10 models. Plots of true versus predicted latitude (a) and longitude (c) indicate better latitude resolution than longitude resolution. Predicted latitude (b) density maps demonstrate the ability to distinguish between the two northernmost locations (PG and JV) from the three southernmost locations (LP, HP, and CR), but offer little discerning power within those two groups. Conversely, predicted longitude (d) density maps show substantial overlap in predicted locations.

Table 3
Confusion Matrix for 10 randomized PLS2-DA classification predictions with the ICP-MS dataset. Each abbreviation corresponds to a given location designated by the HUC12 name and number: Jacksonville (JV, 171003080112), Lithia Park, Ashland (LP, 171003080106), Colestin Road, Colestin (CR, 180102060602), Howard Prairie Resort Campground (HP, 180102060401), and Pelican Guard Station (PG, 180102030203).

		True Location Abbreviation				
Predicted Location Abbreviation	Predicted \ True	CR	HP	LP	JV	PG
	CR	31	0	0	0	0
	HP	1	40	2	0	0
	LP	5	0	35	0	0
	JV	3	0	1	40	0
	PG	0	0	2	0	40

variance explained, respectively. This corresponds to 9-km latitude and 10-km longitude resolution at one standard deviation. Tuned models required ~9 factors for latitude and ~10 factors for longitude, depending on the randomized training set. Plots of predicted versus true latitude (Fig. 4 a) and longitude (Fig. 4 c) show a significant trend across the geospatial coordinates. Density plots for the predicted geolocation for latitude (Fig. 4 b) and longitude (Fig. 4 d) of each class show a clear progression from north to south and east to west but are sufficiently overlapped that no location can be cleanly resolved except for the possible exception of PG in the far north-east.

Variable importance

To better understand the chemical relationship between classification and geolocation, variable importance was assessed for the ICP-MS

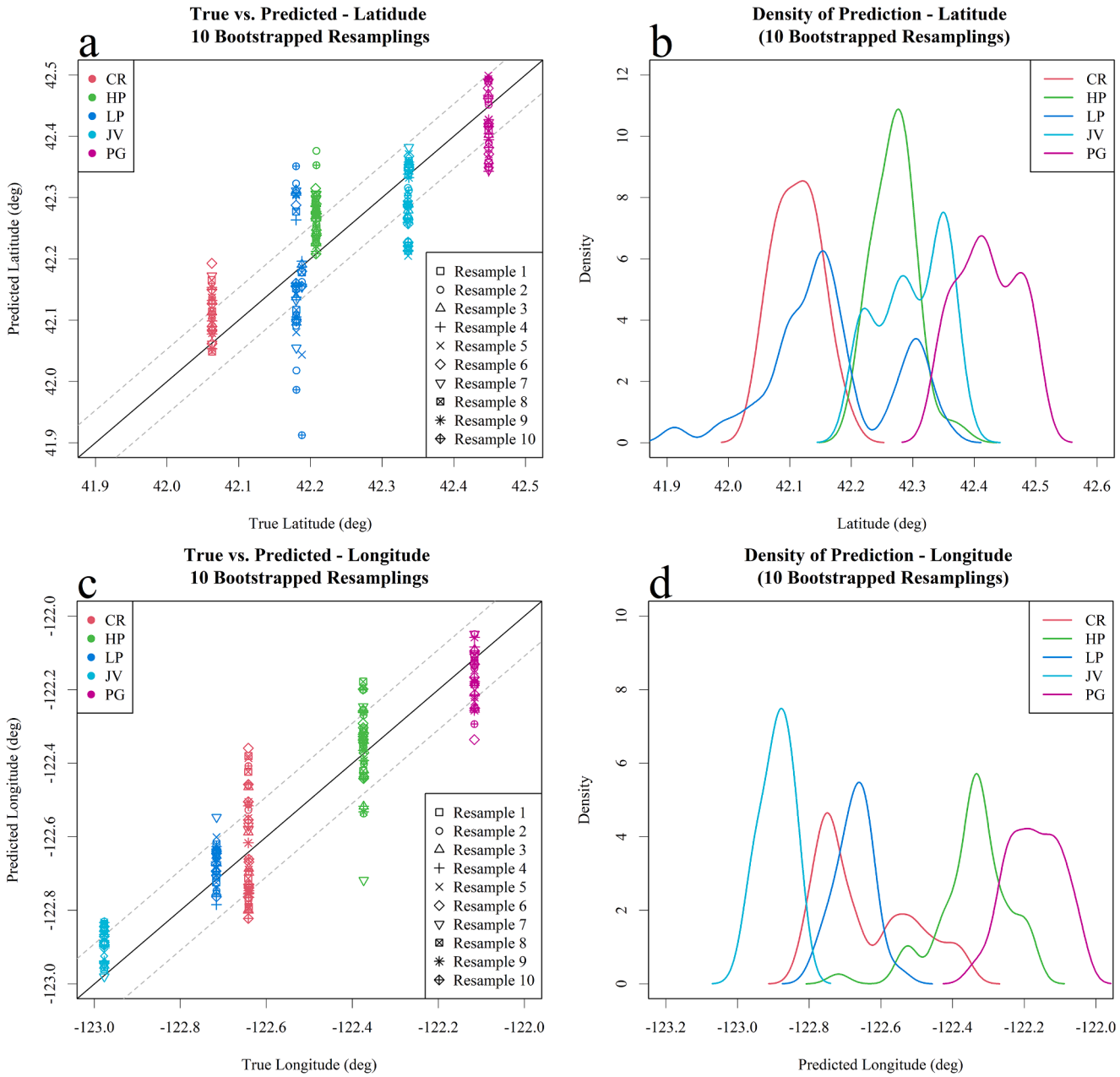


Fig. 3. PLSR models, following a Box-Cox transformation, against latitude and longitude using the ICP-MS data returned RMSEP of 0.08 ± 0.01 and 0.15 ± 0.02, respectively, across 10 randomized calibration models. Plots of predicted versus true latitude (a) and longitude (c) show a significant trend across the geospatial coordinates. However, the density plots of predicted latitude (b) or longitude (d) for each of the five illustrate that the models are truly only able to resolve three locations across the data – near the two extremes or in the middle.

Table 4
Average Confusion Matrix for 10 randomized SVM classification predictions with the LIBS dataset. Each abbreviation corresponds to a given location designated by the HUC12 name and number: Jacksonville (JV, 171003080112); Lithia Park, Ashland (LP, 171003080106); Colestin Road, Colestin (CR, 180102060602); Howard Prairie Resort Campground (HP, 180102060401); and Pelican Guard Station (PG, 180102030203).

		True Location Abbreviation				
Predicted Location Abbreviation	Pred \ True	CR	HP	LP	JV	PG
	CR	43.3	4.8	1.9	0	0
	HP	5.3	44.5	0.2	0	0
	LP	4	0.3	50.1	0.6	0
	JV	0	0	0.9	49.1	0
	PG	0.2	0.3	0	0.7	48.8

and LIBS datasets. Variable importance was not determined for the DART TOFMS data because the chemical interpretation of each peak was unknown and, additionally, the models did not perform as well as the ICP-MS or LIBS data sets. Note, the ICP-MS and LIBS data individually excel at detecting different sets of elements; consequently, these methods would be expected to yield different lists of important variables. While ICP-MS is highly capable of detecting ppb or lower levels of numerous elemental signatures, quadrupole designs like that used in this study typically struggle to detect the organic elements (C, H, N, O, F) as well as some alkali and alkali earths, like K & Ca, due to background interferences, and are thus best at detecting transition metal signatures. On the other hand, LIBS excels at detecting lighter elements (< Kr), including the organic elements, but is capable of detecting nearly all elemental signatures across the periodic table, albeit at notably higher limits of detection relative to ICP-MS. It is because of this detection limit

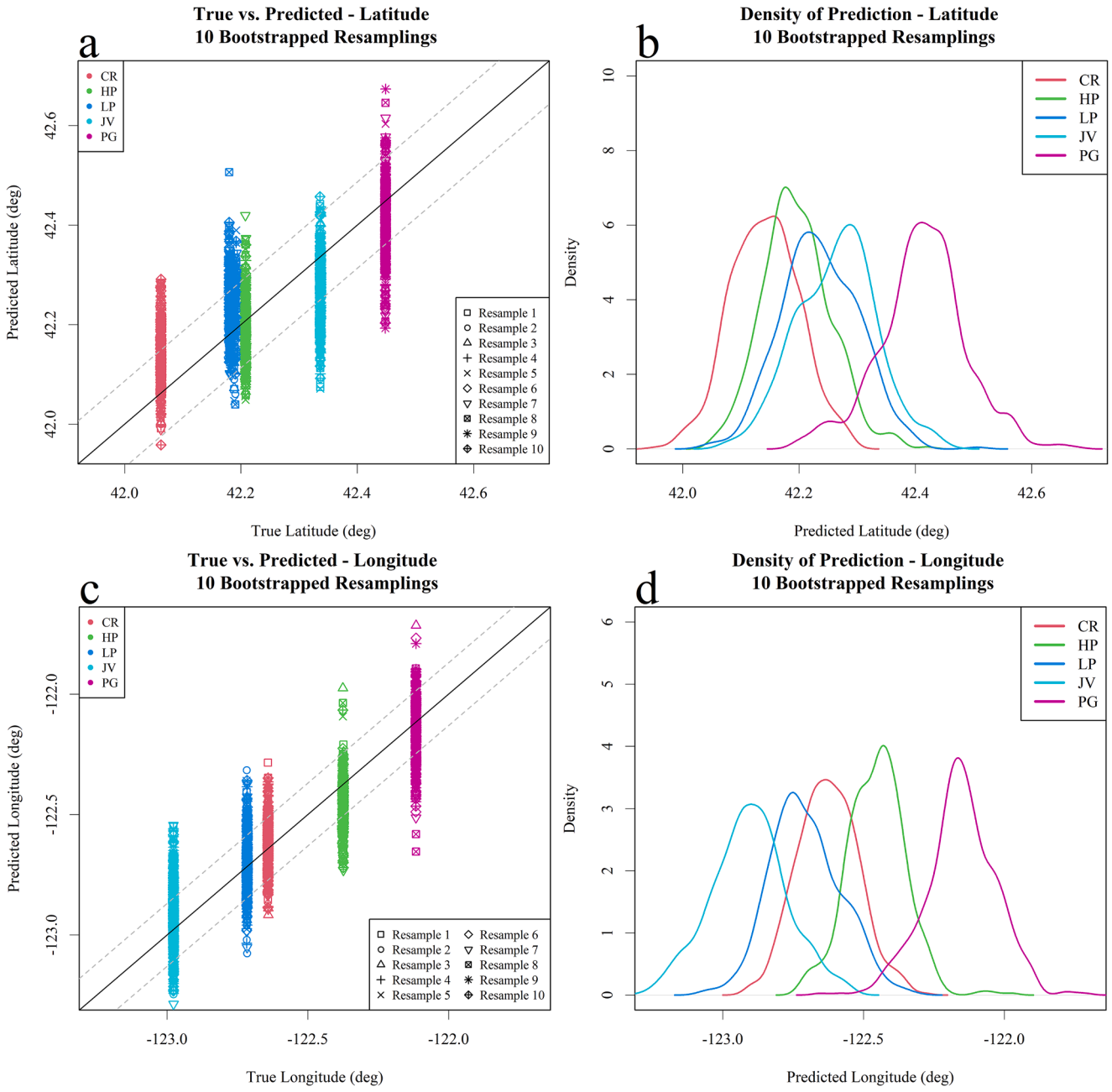


Fig. 4. PLSR models, following normalization to unit standard deviation and unit variance, against latitude and longitude using the LIBS data returned RMSEP of 0.087 ± 0.004 and 0.130 ± 0.004, respectively, across 10 randomized calibration models. Plots of predicted versus true latitude (a) and longitude (c) show a significant trend across the geospatial coordinates. Density plots for the predicted geolocation for latitude (b) and longitude (d) of each class show a clear progression from north to south and east to west, but are sufficiently overlapped that no location can be cleanly resolved with the exception of PG in the far north-east.

discrepancy between the methods that explains the unique sets of elements identified as "most important" for each technique, as outlined below.

Variable importance analyses identified key predictive features in the ICP-MS data. Several mass-to-charge (m/z) ratios fell below detection limits, potentially introducing errors and spurious correlations. To enhance reliability and interpretability, the variables were from 46 to 15 m/z ratios by evaluating detection frequencies and signal intensities, retaining only those with vast preponderance of signals above detection limits. A PCA bi-plot showing the classes distributions and the variable importance for the 46 m/z data and for the 15 m/z is showed in Fig. 5.

The reduction from 46 to 15 m/z variables maintains the class separation in PCA space, suggesting significant collinearity among the original variables. This preservation of data distribution patterns confirms that the selected 15 m/z variables capture the essential geochemical information. The bi-plot reveals distinct chemical signatures across classes - notably, ^{39}K and ^{86}Sr show higher concentrations in the PG class, while ^{59}Co and ^{137}Ba exhibit lower concentrations in the JV class. Similar interpretations can be made for the remaining variables based on their positions and loadings in the bi-plot.

The concept of variable importance extends beyond PCA to the PLS2-DA model, where importance is determined by the model loadings. While PCA loadings reflect each variable's contribution to overall data variance, PLS2-DA loadings provide additional insight by measuring each variable's importance in discriminating between classes. The PLS2-DA loadings incorporate both the variance structure of the predictor variables and their relationship with the response variables, making them particularly valuable for understanding which chemical signatures

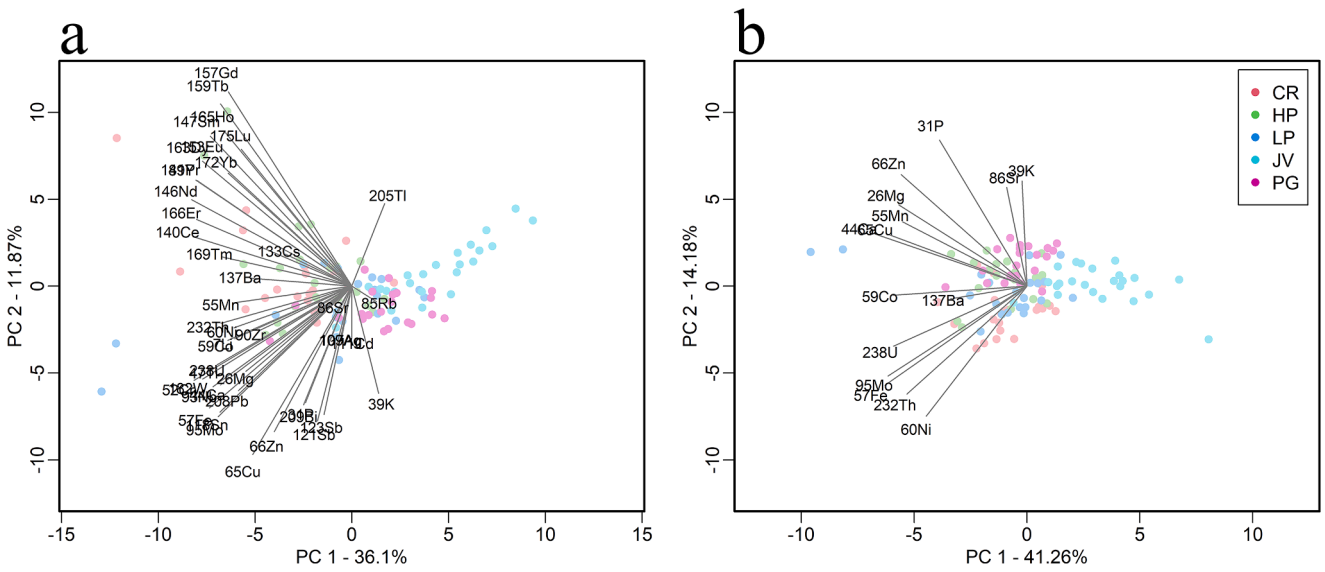


Fig. 5. PCA bi-plots showing class distributions and variable importance for (a) the original 46 m/z variables and (b) the reduced set of 15 m/z variables. The plots demonstrate preserved class separation patterns despite dimensionality reduction, with distinct chemical signatures across sample classes (CR, HP, LP, JV, and PG) indicated by the relative positions and loadings of key elements.

are most useful for distinguishing between sample groups. This supervised approach complements the unsupervised PCA analysis by specifically highlighting variables that drive class separation. Table 5 displays the variables with importance higher than 80% of the maximum variable importance for each class.

The variable importance analysis provides insights into the PLS2-DA model's performance across different classes. Classes JV and PG demonstrate superior classification performance, with 5 and 3 important variables respectively. These multiple distinctive variables provide strong discriminatory power, explaining why no samples from these classes were misclassified in the confusion matrix (Table 3). In contrast, the LV class shows weaker classification performance, with only one distinctive variable (^{86}Sr). This limited discriminatory power explains why five samples from this class were misclassified. An interesting observation emerges when comparing CR and HP classes: despite both having two important variables, their classification accuracies differ significantly. All HP samples were correctly classified, while nine CR samples were misclassified. This discrepancy can be attributed to variable overlap patterns in the chemical signatures. The variable ^{86}Sr serves as an important discriminator for both CR and LV classes, but lacks unique discriminatory power for either class alone. Similarly, ^{66}Zn shows importance across multiple classes (CR, JV, and PG), with particularly high importance for JV and PG. This overlap in discriminatory variables creates a competitive effect where the same chemical marker must serve multiple classification purposes. When a variable like ^{66}Zn is shared across classes but shows stronger importance for certain classes (JV and PG), it can lead to misclassification of samples from classes where it has weaker importance (CR).

A number of similar conclusions can be drawn when assessing LIBS line importance, however, as highlighted above, the elemental signatures used for classification differ substantially from ICP-MS. It should also be noted here that due to the large number of variables (1080) in the LIBS analysis, a bi-plot is an inefficient visualization. Variable importance analyses showed that PLSR models to predict exact longitude or latitude were dominated exclusively by collinear variables composing only 5 LIBS lines: K-766 nm (longitude and latitude), K-769 nm (longitude and latitude), Ca-393 nm (longitude), Ca-397 nm (longitude), and Ca-422 nm (longitude). This focus on K and Ca lines is also seen in both PLS2-DA models across all classes with the LIBS data.

Model-agnostic VIP scores for the LIBS (Table 6) present a similar range of important variables as the other VIP metrics. It can be seen that all elemental lines except for Si are distributed across more than one class, thereby decreasing their discriminatory power for each additional class. JV, the most confidently classified location, shows Mg-285 nm as 9 of its 10 most important variables. PG is the next best predicted class, exhibiting C-247 nm as its most important variable and Mg-285 nm following as the next 11 most important variables. LP, which is still predicted with > 90% accuracy, is dominated by the potassium and oxygen lines. The two worst predicted classes, HP and CR, respectively, can be explained by their repeated use of variables from the other three better-performing classes. That is, HP shares C-247 nm as its most important line and Mg-285 nm as its next 9 variables, while 9 of CR's top 10 variables are potassium and oxygen, all of which clearly aided in increased prediction of other classes. Thus, this competitive behavior can explain why CR & HP are misclassified as one another, despite not sharing any LIBS lines of > 70% importance, further corroborating results seen in the ICP-MS analysis.

Table 5
Variable importance analysis showing key *m/z* ratios (>80% importance relative to the most important variable) for each sample class, listed in decreasing order of importance.

Class	Class Number	Important *m/z*
CR	1	137 (Ba), 66 (Zn)
HP	2	137(Ba), 86 (Sr)
LV	3	86 (Sr)
JV	4	66 (Zn), 95 (Mo), 232 (Th), 238 (U), 59 (Co)
PG	5	66 (Zn), 137 (Ba), 60 (Ni)

Table 6
Variable importance analysis showing key LIBS emission lines (in nm, >70% importance) for each sample class. Approximate wavelengths are reported due to collinearity of neighboring pixels. In most cases, multiple pixels from the same elemental line are of neighboring importance.

Element/Class	CR	HP	LP	JV	PG
C	-	247	247	-	247
Ca	396, 422	-	396, 393	-	-
K	769	-	770, 769	766	-
Mg	280	285	-	285	285
N	-	484	-	-	484
O	776, 777	-	776, 777	-	-
Si	-	-	-	250, 251	-

Discussion

Geolocation models using the DART TOFMS dataset performed significantly worse than the models that used the ICP-MS dataset or the LIBS dataset for the pine samples. The DART TOFMS with a PLS2-DA had a classification accuracy of 0.76 and kappa of 0.70. These performance metrics are respectable but were significantly lower than the performance metrics for ICP-MS with a PLS2-DA accuracy of 0.93 and a kappa of 0.91, and LIBS with an SVM accuracy of 0.92 and a kappa of 0.91 (Table 1). Across the roughly 43-km latitude and 72-km longitude area of this study, plus or minus one standard deviation, of the predicted locations spans 33% of the latitude range and 87% of the longitude range. Plotting the predicted latitude and longitude of each sample generated using the DART TOFMS dataset (Fig. 6 a) shows the ability to differentiate the extreme NE location (PG) and the extreme NW location (JV) from the other three locations (CR, HP, and LP). However, further differentiation as latitude-longitude pairs is not evident.

The relatively poor ability of the DART TOFMS dataset to support accurate and precise geolocation models can be justified by the nature of the molecular measurements. By comparison, ICP-MS and LIBS provide elemental analyses that track native soil composition and hydrology; the *P. ponderosa* trees absorb trace minerals from the soil and groundwater that are evident in the ICP-MS and LIBS measurements [27]. It is reasonable to assume that there is a difference in the molecular composition of the *P. ponderosa* populations as a function of latitude, elevation, and water availability resulting in slight differences in the DART TOF mass spectra from each location [9,11]. Whether the 72-km spread in latitude is sufficient to elucidate a difference in DART TOF mass spectra, or if the demonstrated ability to differentiate latitude is correlated with other factors impacting tree chemistry, is beyond the scope of this study.

Biplots of the predicted latitude and longitude generated using the ICP-MS dataset (Fig. 6 b) and the LIBS dataset (Fig. 6 c) illuminate the abilities of these two methods as tools for use in providing geolocation information of timber origin. While there appears to be more separation between the five classes in Fig. 6 b the LIBS dataset used to generate Fig. 6 c contained 12 times more sample spectra. This leads to a denser Fig. 6 c plot where the classes appear to blend together more than the Fig. 6 b plot, though models using ICP-MS data and LIBS data return comparable classification performance metrics and the predictive accuracy and kappa values are numerically identical within the standard deviation of the bootstrap. Similarly, the two methods' RMSEP of latitudes were numerically identical within the standard deviation of the bootstrap. However, with respect to longitude, the 0.12 RMSEP for the

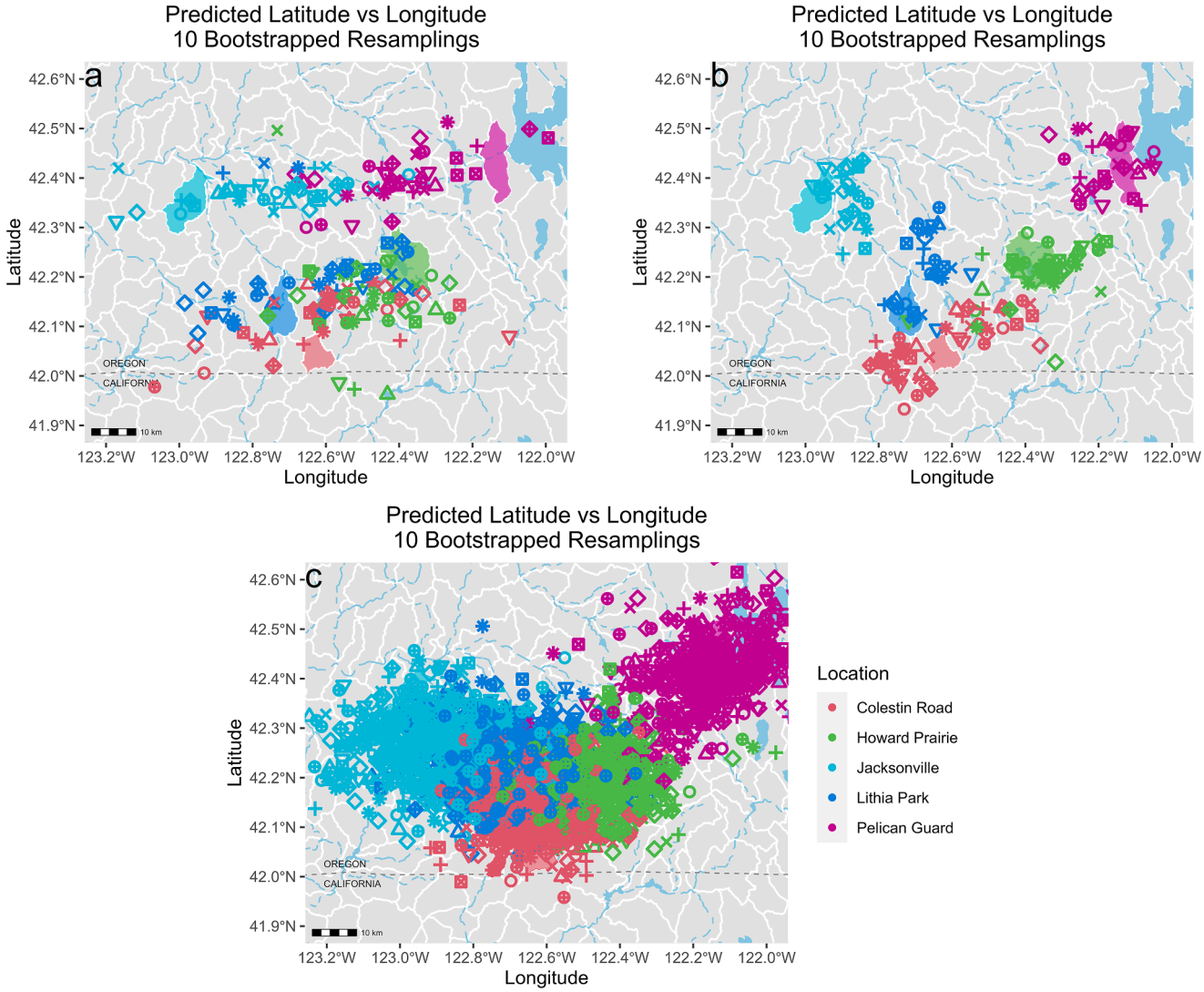


Fig. 6. Predicted latitude and longitude of each sample. Biplots of the predicted latitude and longitude for DART TOFMS (a), ICP-MS (b), and LIBS (c). The predicted longitude and latitudes from each instrument indicate that: DART TOFMS can differentiate the extreme northeast location (PG) and extreme northwest location (JV) from the other three locations (CR, HP, and LP), while ICP-MS and LIBS can provide geolocation information of timber origin in both longitude and latitude.

model using LIBS data is statistically different from the 0.15 RMSEP for the model using ICP-MS data ($p = 0.02$).

The analysis using LIBS data has significantly less variance in the bootstrapped accuracy and kappa than ICP-MS (0.02 vs 0.07), but this is likely the result of the LIBS spectra data being trained with 12 times more samples than ICP-MS spectra per *P. ponderosa* core sample leading to a much more stable model. The inhomogeneity of the tree cores also essentially led to each LIBS spectrum being an independent sample because it samples different 1 – 2 growth-year portions of the core. By comparison, digesting the cores for ICP-MS homogenized the core samples across multiple growth rings.

The comparable performances of models using ICP-MS data and LIBS data demonstrates that LIBS is a viable and intriguing alternative to ICP-MS analyses to create databases for identification of wood provenance. ICP-MS is a relatively intensive technique in terms of money, labor, and reagents. In addition, an ICP-MS is an expensive laboratory instrument and samples must be converted to ash and dissolved in high purity acid prior to analysis with turn-around time for an ICP-MS sample a minimum of 12 hr. Alternatively, LIBS spectra were collected with a handheld, field-portable instrument initially designed for use by welders and machinists. No sample preparation is needed for LIBS data collection and a single sample can be analyzed at multiple locations with replicates in under two minutes. This research indicates the possibility for LIBS to supply rapid analyses of larger collections of data in the field and with better statistical coverage than traditional ICP-MS based experimental designs.

While variable importance is a key metric for understanding the complex interplay of input variables to model performance, there are still limitations associated with them, including that they don't allow for a mechanistic understanding of a given model, and that precise variable importance is impossible to calculate for some models. Beyond these limitations, as was previously stated, variable importance assumes that models are properly trained, tuned, and cross validated, and are inherently limited to the variables contained within the analysis. This, then, leaves an open question to further explore the complex biological and chemical interplay that leads to bioavailability of micronutrients through synergism and antagonism, and how this subtle effect relates to local geology, however, this analysis is outside the scope of this study.

Conclusion

Using the three methods described above, we were able to collect both molecular and elemental information. Outside of the scope of this research is whether geographic differences are based on genetics, which could be detected via molecular data, or environmental influences, which could be detected via elemental data, or a mixture of both. While the results of ICP-MS could indicate that environmental differences are the basis for geographic signals, we cannot know for sure that these elemental differences are also the drivers for differences found in the LIBS spectral data or the DART TOF mass spectra. However, this study showed that the chemical composition of five populations of *P. ponderosa* had changed sufficiently within distances of 14 to 72 km to allow for their separation via chemometrics across three different techniques. PLS2-DA applied to DART TOF mass spectra resolved the *P. ponderosa* populations with a validation accuracy of 76% and a kappa value of 70%, while PLS2-DA applied to ICP-MS data resulted in a validation accuracy of 93% and a kappa value of 91%. The best performing model for the LIBS spectra was SVM with a validation accuracy of 92% and a kappa value of 91%. While the ICP-MS and LIBS analyses of the *P. ponderosa* samples were superior with errors of less than 10%, the error in each model could likely be addressed through the application of more rigorous data pre-processing steps than applied here, as well as the application of multilevel models.

In conclusion, this research effort provides an additional case study for the continued expansion of DART TOFMS databases for use in geographic provenance identification of timber for larger spatial regions, and it further indicates that trace elemental analysis via ICP-MS is a promising method for use in creating databases to be used to identify the provenance of timber. In addition, the results from the model generated using the LIBS analyzer dataset indicate that geographic signals can be collected with instruments that are relatively inexpensive, fast, and field-deployable, and we expect it to be at the forefront of timber origin identification in the coming years.

CRediT authorship contribution statement

Erin R. Price: Writing – review & editing, Writing – original draft, Supervision, Methodology, Investigation, Formal analysis, Data curation, Conceptualization. **Kierra R. Cano:** Writing – review & editing, Writing – original draft, Methodology, Data curation. **Caelin P. Celani:** Writing – review & editing, Validation, Methodology, Formal analysis, Data curation. **Helder V. Carneiro:** Writing – original draft, Methodology, Formal analysis, Data curation. **Karl S. Booksh:** Writing – original draft, Supervision, Methodology, Formal analysis, Data curation. **James A. Jordan:** Formal analysis, Conceptualization. **Pamela J. McClure:** Writing – review & editing, Methodology, Conceptualization. **Megahn H. Pinedo:** Writing – original draft, Data curation. **Michael E. Ketterer:** Data curation. **Kent M. Elliott:** Writing – review & editing. **Tyler B. Coplen:** Conceptualization. **Edgard O. Espinoza:** Writing – original draft, Supervision, Methodology, Investigation, Data curation, Conceptualization.

Declaration of competing interest

The authors declare that they have no known competing financial interests or personal relationships that could have appeared to influence the work reported in this paper.

Acknowledgements

Any use of trade, firm, or product names is for descriptive purposes only and does not imply endorsement by the U.S. Government. The findings and conclusions in this article are those of the authors and do not represent the views of the U.S. Fish and Wildlife Service or the U.S. Forest Service. The authors would like to thank Jacquelin Green and Lauren T. Reid of the U.S. Geological Survey for their thoughtful and thorough reviews of the manuscript.

Supplementary materials

Supplementary material associated with this article can be found at 10.2737/RDS-2025-0009.

Data availability

Data Statment section at the end of the manuscript contains the DOI for the data repo where all data are shared. Please see Reviewer Response document for the current and temporary location of data https://doi.org/10.2737/RDS-2025-0009.

References

[1] J.P. Prestemon, J. Buongiorno, D.N. Wear, J.P. Siry, International Trade In Forest Products, in: 2003: pp. 177–199. doi:10.1007/978-94-017-0219-5_11.
[2] C.M.T. Johnston, J. Guo, J.P. Prestemon, Forest Products, 2023. doi:10.2737/WO-GTR-102-Chap7.
[3] J.P. Prestemon, The impacts of the Lacey Act Amendment of 2008 on U.S. hardwood lumber and hardwood plywood imports, For. Policy. Econ. 50 (2015) 31–44, https://doi.org/10.1016/j.forpol.2014.10.002.
[4] A.E. Johnson, D. Gehl, The 2008 "Illegal Logging Amendments", Natural Resources & Environment 33 (2019) 38–42. https://www.jstor.org/stable/27010505.
[5] M. Köthke, M. Lippe, P. Elsasser, Comparing the former EUTR and upcoming EUDR: Some implications for private sector and authorities, For. Policy. Econ. 157 (2023) 103079, https://doi.org/10.1016/j.forpol.2023.103079.

[6] R.N. Kigathi, W.W. Weisser, M. Reichelt, J. Gershenzon, S.B. Unsicker, Plant volatile emission depends on the species composition of the neighboring plant community, BMC. Plant Biol. 19 (2019) 58, https://doi.org/10.1186/s12870-018-1541-9.

[7] J.K. Holopainen, V. Virjamo, R.P. Ghimire, J.D. Blande, R. Julkunen-Tiitto, M. Kivimäenpää, Climate Change Effects on Secondary Compounds of Forest Trees in the Northern Hemisphere, Front. Plant Sci. 9 (2018), https://doi.org/10.3389/fpls.2018.01445.

[8] K. Keefover-Ring, Y.B. Linhart, Variable Chemistry and Herbivory of Ponderosa Pine Cones, Int. J. Plant Sci. 171 (2010) 293–302, https://doi.org/10.1086/650155.

[9] A.E. Squillace, Geographic Variation in Slash Pine, Forest Science 12 (1966) a0001–z0001, https://doi.org/10.1093/forestscience/12.s1.a0001.

[10] Z.V. Stepanov, E.V. Dubovenko, Izvestiya SO AN USSR, Izvestiya Akademii Nauk Turkmenskoi SSR 2 (1971).

[11] A.D. Rogachev, N.F. Salakhutdinov, Chemical Composition of Pinus sibirica (Pinaceae), Chem. Biodivers. 12 (2015) 1–53, https://doi.org/10.1002/cbdv.201300195.

[12] E. Zavarin, K. Snajberk, J. Fisher, Geographic variability of monoterpenes from cortex of Abies concolor, Biochem. Syst. Ecol. 3 (1975) 191–203, https://doi.org/10.1016/0305-1978(75)90002-2.

[13] R.C. Cronn, K.N. Finch, L.L. Hauck, M. Parker-Forney, B.G. Milligan, J. Dowling, A. Scientists, Range-wide assessment of a SNP panel for individualization and geolocalization of bigleaf maple (Acer macrophyllum Pursh), Forensic Science International: Animals and Environments 1 (2021) 100033, https://doi.org/10.1016/j.fsiae.2021.100033.

[14] K.N. Finch, R.C. Cronn, M.C. Ayala Richter, C. Blanc-Jolivet, M.C. Correa Guerrero, L. De Stefano Beltrán, C.R. García-Dávila, E.N. Honorio Coronado, S. Palacios-Ramos, K. Paredes-Villanueva, F.A. Jones, Predicting the geographic origin of Spanish Cedar (Cedrela odorata L.) based on DNA variation, Conservation Genetics 21 (2020) 625–639, https://doi.org/10.1007/s10592-020-01282-6.

[15] T. Mortier, J. Truszkowski, M. Norman, M. Boner, B. Buliga, C. Chater, H. Jennings, J. Saunders, R. Sibley, A. Antonelli, W. Waegeman, V. Deklerck, A framework for tracing timber following the Ukraine invasion, Nat. Plants. 10 (2024) 390–401, https://doi.org/10.1038/s41477-024-01648-5.

[16] C.J. Watkinson, G.O. Rees, M.C. Gwenael, P. Gasson, S. Hofem, L. Michely, M. Boner, Stable Isotope Ratio Analysis for the Comparison of Timber From Two Forest Concessions in Gabon, Front. For. Glob. Change 4 (2022), https://doi.org/10.3389/ffgc.2021.650257.

[17] A. Kagawa, S.W. Leavitt, Stable carbon isotopes of tree rings as a tool to pinpoint the geographic origin of timber, Journal of Wood Science 56 (2010) 175–183, https://doi.org/10.1007/s10086-009-1085-6.

[18] W.M. Rhodes, D. Ph, E.P. Allen, M. Callahan, Illegal logging: A market-based analysis of trafficking in illegal timber, Trends. Organ. Crime 10 (2006) 61–64, https://doi.org/10.1007/s12117-006-1030-7.

[19] E. Sisco, T.P. Forbes, Forensic applications of DART-MS: A review of recent literature, Forensic Chemistry 22 (2021) 100294, https://doi.org/10.1016/j.forc.2020.100294.

[20] E.R. Price, I. Miles-Bunch, P.E. Gasson, C.A. Lancaster, Inference of origin of Pterocarpus timber by chemical profiling of ambient ionization mass spectra, Forensic Science International: Animals and Environments 1 (2021) 100032, https://doi.org/10.1016/j.fsiae.2021.100032.

[21] V. Deklerck, C.A. Lancaster, J. Van Acker, E.O. Espinoza, J. Van den Bulcke, H. Beeckman, Chemical Fingerprinting of Wood Sampled along a Pith-to-Bark Gradient for Individual Comparison and Provenance Identification, Forests. 11 (2020) 107, https://doi.org/10.3390/f11010107.

[22] K. Finch, E. Espinoza, F.A. Jones, R. Cronn, Source identification of western Oregon Douglas-fir wood cores using mass spectrometry and random forest classification, Appl. Plant Sci. 5 (2017), https://doi.org/10.3732/apps.1600158.

[23] H. Lachas, R. Richaud, A.A. Herod, D.R. Dugwell, R. Kandiyoti, Determination of trace elements by inductively coupled plasma mass spectrometry of biomass and fuel oil reference materials using milligram sample sizes, Rapid Communications in Mass Spectrometry 14 (2000) 335–343, https://doi.org/10.1002/(SICI)1097-0231(20000315)14:5<335::AID-RCM854>3.0.CO;2-0.

[24] C. Durante, C. Baschieri, L. Bertacchini, M. Cocchi, S. Sighinolfi, M. Silvestri, A. Marchetti, Geographical traceability based on 87Sr/86Sr indicator: A first approach for PDO Lambrusco wines from Modena, Food Chem. 141 (2013) 2779–2787, https://doi.org/10.1016/j.foodchem.2013.05.108.

[25] E.C. Mazarakioti, A. Zotos, A.-A. Thomatou, A. Kontogeorgos, A. Patakas, A. Ladavos, Inductively Coupled Plasma-Mass Spectrometry (ICP-MS), a Useful Tool in Authenticity of Agricultural Products' and Foods' Origin, Foods. 11 (2022) 3705, https://doi.org/10.3390/foods11223705.

[26] M.G. Alaimo, A. Saitta, E. Ambrosio, Bedrock and soil geochemistry influence the content of chemical elements in wild edible mushrooms (Morchella group) from South Italy (Sicily), Acta Mycol 54 (2019), https://doi.org/10.5586/am.1122.

[27] L.E. Boeschoten, U. Sass-Klaassen, M. Vlam, R.N.J. Comans, G.F. Koopmans, B.R. V. Meyer-Sand, S.N. Tassiamba, M.T. Tchamba, H.T. Zanguim, P.T. Zemtsa, P. A. Zuidema, Clay and soil organic matter drive wood multi-elemental composition of a tropical tree species: Implications for timber tracing, Science of The Total Environment 849 (2022) 157877, https://doi.org/10.1016/j.scitotenv.2022.157877.

[28] P. Seidel, D. Ebert, R. Schinke, R. Möckel, S. Raatz, M. Chao, E. Niederschlag, T. Kreschel, R. Gloaguen, A.D. Renno, Comparison of Elemental Analysis Techniques for the Characterization of Commercial Alloys, Metals. (Basel) 11 (2021) 736, https://doi.org/10.3390/met11050736.

[29] A. Syuhada Mangsor, Z. Haider Rizvi, K. Chaudhary, M.Safwan Aziz, Classification of alloys using laser induced breakdown spectroscopy with principle component analysis, J. Phys. Conf. Ser. 1027 (2018) 012017, https://doi.org/10.1088/1742-6596/1027/1/012017.

[30] P. Inakollu, T. Philip, A.K. Rai, F.-Y. Yueh, J.P. Singh, A comparative study of laser induced breakdown spectroscopy analysis for element concentrations in aluminum alloy using artificial neural networks and calibration methods, Spectrochim. Acta Part B At. Spectrosc. 64 (2009) 99–104, https://doi.org/10.1016/j.sab.2008.11.001.

[31] C. Fabre, Advances in Laser-Induced Breakdown Spectroscopy analysis for geology: A critical review, Spectrochim. Acta Part B At. Spectrosc. 166 (2020) 105799, https://doi.org/10.1016/j.sab.2020.105799.

[32] N.J. McMillan, S. Rees, K. Kochelek, C. McManus, Geological Applications of Laser-Induced Breakdown Spectroscopy, Geostand. Geoanal. Res. 38 (2014) 329–343, https://doi.org/10.1111/j.1751-908X.2014.00308.x.

[33] M.E. Essington, G.V. Melnichenko, M.A. Stewart, R.A. Hull, Soil Metals Analysis Using Laser-Induced Breakdown Spectroscopy (LIBS), Soil Science Society of America Journal 73 (2009) 1469–1478, https://doi.org/10.2136/sssaj2008.0267.

[34] D. Riebe, A. Erler, P. Brinkmann, T. Beitz, H.-G. Löhmannsröben, R. Gebbers, Comparison of Calibration Approaches in Laser-Induced Breakdown Spectroscopy for Proximal Soil Sensing in Precision Agriculture, Sensors 19 (2019) 5244, https://doi.org/10.3390/s19235244.

[35] Y. Xu, B. Han, X. Tan, Q. Jiao, Z. Ma, B. Lv, Y. Li, H. Li, Y. Zou, L. Yang, Establishment and evaluation of a quantitative analysis model for potentially toxic metals in wet soil samples by LIBS, Eur. J. Soil. Sci. 73 (2022), https://doi.org/10.1111/ejss.13213.

[36] R. Harmon, C. Lawley, J. Watts, C. Harraden, A. Somers, R. Hark, Laser-Induced Breakdown Spectroscopy—An Emerging Analytical Tool for Mineral Exploration, Minerals 9 (2019) 718, https://doi.org/10.3390/min9120718.

[37] G.G. Arantes de Carvalho, M.B. Bueno Guerra, A. Adame, C.S. Nomura, P. V. Oliveira, H.W. Pereira de Carvalho, D. Santos, L.C. Nunes, F.J. Krug, Recent advances in LIBS and XRF for the analysis of plants, J. Anal. At. Spectrom. 33 (2018) 919–944, https://doi.org/10.1039/C7JA00293A.

[38] D. Santos, L.C. Nunes, G.G.A. de Carvalho, M.da S. Gomes, P.F. de Souza, F.de O. Leme, L.G.C. dos Santos, F.J. Krug, Laser-induced breakdown spectroscopy for analysis of plant materials: A review, Spectrochim. Acta Part B At. Spectrosc. 71–72 (2012) 3–13, https://doi.org/10.1016/j.sab.2012.05.005.

[39] C.P. Celani, C.A. Lancaster, J.A. Jordan, E.O. Espinoza, K.S. Booksh, Assessing utility of handheld laser induced breakdown spectroscopy as a means of Dalbergia speciation, Analyst 144 (2019) 5117–5126, https://doi.org/10.1039/C9AN00984A.

[40] N. Baskali-Bouregaa, M.-L. Milliand, S. Mauffrey, E. Chabert, M. Forrestier, N. Gilon, Tea geographical origin explained by LIBS elemental profile combined to isotopic information, Talanta 211 (2020) 120674, https://doi.org/10.1016/j.talanta.2019.120674.

[41] N. Gyftokostas, D. Stefas, S. Couris, Olive Oils Classification via Laser-Induced Breakdown Spectroscopy, Applied Sciences 10 (2020) 3462, https://doi.org/10.3390/app10103462.

[42] M.M. El-Deftar, J. Robertson, S. Foster, C. Lennard, Evaluation of elemental profiling methods, including laser-induced breakdown spectroscopy (LIBS), for the differentiation of Cannabis plant material grown in different nutrient solutions, Forensic Sci. Int. 251 (2015) 95–106, https://doi.org/10.1016/j.forsciint.2015.03.029.

[43] A. Willyard, D.S. Gernandt, K. Potter, V. Hipkins, P. Marquardt, M.F. Mahalovich, S.K. Langer, F.W. Telewski, B. Cooper, C. Douglas, K. Finch, H.H. Karemera, J. Lefler, P. Lea, A. Wofford, Pinus ponderosa : A checkered past obscured four species, Am. J. Bot. 104 (2017) 161–181, https://doi.org/10.3732/ajb.1600336.

[44] R. Smith, Xylem monoterpenes of pines: distribution, variation, genetics, function, U.S. Department of Agriculture, Forest Service, Pacific Southwest Research Station, 2000. doi:10.2737/psw-gtr-177.

[45] The National Map Viewer, U.S. Geological Survey (2022). https://apps.nationalmap.gov/viewer/.

[46] P.J. McClure, G.D. Chavarria, E. Espinoza, Metabolic chemotypes of CITES protected Dalbergia timbers from Africa, Madagascar, and Asia, Rapid, Communications in Mass Spectrometry 29 (2015) 783–788, https://doi.org/10.1002/rcm.7163.

[47] JEOL, MsAxel Data Processing LP v. 1.05.2, (2018), JEOL Ltd., 2018.

[48] R Core Team, R: A Language and Environment for Statistical Computing, (2020). https://www.r-project.org/.

[49] RStudio Team, RStudio: Integrated Development Environment for R, (2020). http://www.rstudio.com/.

[50] M. Kuhn, caret: Classification and Regression Training (R package version 6.0-86), (2020). https://cran.r-project.org/package=caret.

[51] S. Corporation, Microsoft; Weston, doParallel: Foreach Parallel Adaptor for the "parallel" Package (R package version 1.0.16), (2020). https://cran.r-project.org/package=doParallel.

[52] Signal Developers, signal: Signal processing, (2014). http://r-forge.r-project.org/projects/signal/.

[53] J. Wickham, H.; Bryan, readxl: Read Excel Files (R package version 1.4.3), (2023). https://cran.r-project.org/package=readxl.

[54] K.H. Liland, T. Almøy, B.-H. Mevik, Optimal Choice of Baseline Correction for Multivariate Calibration of Spectra, Appl. Spectrosc. 64 (2010) 1007–1016, https://doi.org/10.1366/000370210792434350.

[55] H. Kim, discretization: Data Preprocessing, Discretization for Classification (R package version 1.0-1.1), (2022). https://cran.r-project.org/package=discretization.

[56] D. Wickham, Hadley; François, Romain; Henry, Lionel; Müller, Kirill; Vaughan, Dplyr: A Grammar of Data Manipulation, (2020). https://cran.r-project.org/package=dplyr.
[57] G.E.P. Box, D.R. Cox, An Analysis of Transformations, J. R. Stat. Soc. Series. B Stat. Methodol. 26 (1964) 211–243, https://doi.org/10.1111/j.2517-6161.1964.tb00553.x.
[58] W.N. Venables, B.D. Ripley, Modern Applied Statistics with S, Springer New York, New York, NY, 2002. doi:10.1007/978-0-387-21706-2.
[59] L.A. Kurgan, K.J. Cios, CAIM discretization algorithm, IEEe Trans. Knowl. Data Eng. 16 (2004) 145–153, https://doi.org/10.1109/TKDE.2004.1269594.
[60] J.A. Jordan, C.P. Celani, M. Ketterer, B.K. Lavine, K.S. Booksh, Supervised discretization for decluttering classification models, Analyst 148 (2023) 6097–6108, https://doi.org/10.1039/D3AN00770G.
[61] C.D. Bernardes, P.J.S. Barbeira, Different Chemometric Methods for the Discrimination of Commercial Aged Cachaças, Food Anal. Methods 9 (2016) 1053–1059, https://doi.org/10.1007/s12161-015-0284-6.
[62] A.Ya. Chervonenkis, Early History of Support Vector Machines, in: Empirical Inference, Springer Berlin Heidelberg, Berlin, Heidelberg, 2013: pp. 13–20. doi:10.1007/978-3-642-41136-6_3.
[63] B.M. Greenwell, B.C. Boehmke, Variable Importance Plots—An Introduction to the vip Package, R Journal 12 (2020) 343–366, https://doi.org/10.32614/rj-2020-013.
[64] M. Kuhn, K. Johnson, Applied Predictive Modeling, Springer New York, New York, NY, 2013. doi:10.1007/978-1-4614-6849-3.
[65] S. Probst, Philipp; Janitza, Package "varImp", (2020). https://cran.r-project.org/web/packages/varImp/index.html.
[66] T.R. Nichols, P.M. Wisner, G. Cripe, L. Gulabchand, Putting the Kappa Statistic to Use, The Quality Assurance Journal 13 (2010) 57–61, https://doi.org/10.1002/qaj.481.